International Journal of Occupational Safety and Ergonomics

ISSN: 1080-3548 (Print) 2376-9130 (Online) Journal homepage: http://www.tandfonline.com/loi/tose20

Experimental investigation of biodynamic human body models subjected to whole-body vibration during a vehicle ride

Yener Taskin, Yuksel Hacioglu, Faruk Ortes, Derya Karabulut & Yunus Ziya Arslan

To cite this article: Yener Taskin, Yuksel Hacioglu, Faruk Ortes, Derya Karabulut & Yunus Ziya Arslan (2018): Experimental investigation of biodynamic human body models subjected to whole-body vibration during a vehicle ride, International Journal of Occupational Safety and Ergonomics, DOI: 10.1080/10803548.2017.1418487

To link to this article: https://doi.org/10.1080/10803548.2017.1418487

Accepted author version posted online: 18 Dec 2017.
Published online: 06 Feb 2018.

International Journal of Occupational Safety and Ergonomics (JOSE), 2018
https://doi.org/10.1080/10803548.2017.1418487

Experimental investigation of biodynamic human body models subjected to whole-body vibration during a vehicle ride

Yener Taskin, Yuksel Hacioglu, Faruk Ortes, Derya Karabulut and Yunus Ziya Arslan *

Faculty of Engineering, Istanbul University, Turkey

In this study, responses of biodynamic human body models to whole-body vibration during a vehicle ride were investigated. Accelerations were acquired from three different body parts, such as the head, upper torso and lower torso, of 10 seated passengers during a car ride while two different road conditions were considered. The same multipurpose vehicle was used during all experiments. Additionally, by two widely used biodynamic models in the literature, a set of simulations were run to obtain theoretical accelerations of the models and were compared with those obtained experimentally. To sustain a quantified comparison between experimental and theoretical approaches, the root mean square acceleration and acceleration spectral density were calculated. Time and frequency responses of the models demonstrated that neither of the models showed the best prediction performance of the human body behaviour in all cases, indicating that further models are required for better prediction of the human body responses.

Keywords: human body modelling; lumped-parameter models; seated human subjects; whole-body vibration

1. Introduction

The human body is highly sensitive to vibration effects coming from the environment due to many different causes [1,2]. Vibrations affecting the human body produce discomfort and prevent human body segments such as articulated limbs, legs and arms, head and torso from working in their optimal conditions [3]. Furthermore, degenerative consequences may emerge in the human body as a result of relatively long time exposure to vibrations coming from undesired external excitations. Primarily, lower back pain and disorders, and degenerative disorders of the whole spine (i.e., osteophytes in vertebral discs), especially occupational disease, sciatic pain and alterations in peripheral nervous system function, were reported previously as remarkable and adverse effects of long-lasting vibrations [4–8]. Moreover, there are numerous, secondary, undesirable outputs of these long-term varying stimulations, such as balance and postural disorders, vestibular disturbances, muscle fatigue and respiratory, cardiovascular and also digestive problems [9–13].

The biodynamic response of the human body under whole-body vibration (WBV) has been investigated repeatedly [14–17]. Further, in order to mimic human body behaviours, various human body models were proposed. In these studies, researchers aimed at designing ergonomic seats [18,19] and comfortable vehicle suspensions [20], developing systems that enable reduction of the adverse effects on vehicle occupants in case of frontal crashes, and also perceiving and preventing inconvenient consequences of occupational vibrations coming from different directions [21–23].

Biodynamic or so-called lumped-parameter human body models were employed to observe, test and simulate the effects of WBV, which likely reduces comfort and also causes injury in the case of severe excitations. Human body segments such as the head, torso, arm, etc. are considered as concentrated masses and linked to each other with springs and dampers, taking into account the physical and viscoelastic properties of such living segments [24]. These lumped-parameter models have been proposed with varying degrees of freedom including vertical and horizontal directions [25,26]. The models are beneficial to reach appropriate design and proper tuning of vehicle and seat suspensions especially for seated drivers and occupants. In addition to the models that are intended to represent the anatomical and physiological characteristics of the human body, vehicle design and vehicle–road and human–vehicle interactions are also thought to be influential factors in the realistic simulation of the degenerative effects of vibrations on the human body [27,28]. There has been a significant amount of research including the properties of biodynamic models [29–36]. Qassem et al. [32], Wan and Schimmels [34], Wei and Griffin [37] and Liang and Chiang [24] conducted prominent studies and presented inclusive surveys. For vehicles, WBV effects come from the road on which the vehicle travels, and the surface roughness is a crucial

*Corresponding author. Email: yzarslan@istanbul.edu.tr

parameter in occurrence of the adverse effect of vibration. Biodynamic models are quite practical and an effective tool to simulate WBV with different road conditions. Especially, the models proposed by Boileau and Rakheja [27] and Qassem et al. [32], which were developed according to experimental data recorded from human subjects during different excitation conditions, were widely used to simulate human body behaviour against WBV. Various studies [38–43] employed these two models to elucidate the effects of vibrations on the human body for both experimental and biodynamic model simulation works.

This study aimed to present a comparative and quantitative assessment of widely used lumped-parameter human body models which were suggested and applied to simulate different occupational cases. In order to accomplish this task, acceleration measurements from different body segments of subjects were acquired during a car ride for varying road conditions relating to the road surface roughness level. Furthermore, theoretical accelerations were calculated from the investigated biodynamic models to make a representative comparison between experimental and theoretical results. The root mean square (rms) and power spectral density (PSD) of accelerations for different body segments, i.e., head, lower torso and upper torso, were then calculated to complete the comparison progress in a quantitative manner.

The study also intended to provide an inclusive perspective to conceive whether the existing human body models sufficiently reflect the real human body biodynamic characteristics and allow them to be simulated in a precise and accurate way.

2. Materials and methods

2.1. *Human body models*

Lumped-parameter human body biodynamic models that are composed of rheological elements, such as spring, damper and mass, are practical tools to gain insight into how vibrations from the ground or vehicles would influence the seated occupants. Governing equations, which imply the response of the system, are built according to linkage, order and organization of these simplified elements relating to assumptions for model construction [24].

Although there has been a wide range of such lumped-parameter models in terms of complexity, in this study two commonly used biodynamic models were considered and evaluated in terms of representing the response of the real human body under WBV. These models were proposed by Boileau and Rakheja [27] and Qassem et al. [32], and are referred to as Model 1 and Model 2, respectively (Figure 1). Model 1 and Model 2 have 4 and 11 degrees of freedom, respectively.

Since the biodynamic models include the human–seat interface and the subjects were considered in a sitting position without a backrest, the excitation inputs (or external disturbance) z_0 were assumed to originate from the seat mass. In the models, the stiffness coefficient of the spring element, coefficient of damping element, mass and displacement of the related body segments were represented by k_i, c_i, m_i and z_i, respectively. Numerical values of the model parameters are presented in Appendix 1.

Boileau and Rakheja [27] developed their model (Model 1) since they considered that the previous biodynamic models did not meet the biodynamic response data obtained experimentally under the typical vehicle driving conditions. They estimated their proposed model parameters by correlating the vertical driving-point mechanical impedance and seat-to-head transmissibility response characteristics obtained from the model with the experimental values for drivers maintaining a sitting erect position without backrest support. They employed linear elastic and damping elements, since they assumed the linearity of the system in view of their experimental findings that the driving-point mechanical impedance did not vary significantly over the frequency range of 0.625–10 Hz with excitation amplitudes ranging from 1.0 to 2.0 m/s^2 using a whole-body vehicular vibration simulator. They integrated four masses into their model representing the head and neck, the chest and upper torso, the lower torso and the thighs and pelvis in contact with the seat. They did not include the masses of the lower legs and feet since they assumed that these body segments contributed a negligible amount of biodynamic response of the seated body.

Qassem et al. [32] implemented their lumped-parameter human body model (Model 2), which includes masses representing the lower arm, upper arm, cervical spine, head, torso, thorax, diaphragm, abdomen, thoracic spine, lumbar spine and pelvis, by modifying the model proposed by Muksian and Nash [30–33]. Unlike the Muksian and Nash model, the modified model included the damping and elasticity constants of more body segments, namely the upper and lower arms and cervical, thoracic and lumbar spine. The numerical values of the spring and dashpot elements were drawn from the literature.

2.2. *Experimental protocol*

A series of vibration measurements regarding the predefined experimental protocol were carried out to obtain experimental WBV acceleration data from different segments of the human body. Acceleration measurements were performed with a group of 10 healthy male subjects, for whom ages and masses are presented in Table 1. Safety precautions and measurements were in accordance with Standard No. ISO 13090-1:1998 [44]. Before initiation of the measurement procedure, subjects were given sufficient information about the study and their written consents were taken. None of the subjects reported any previous chronic health problem.

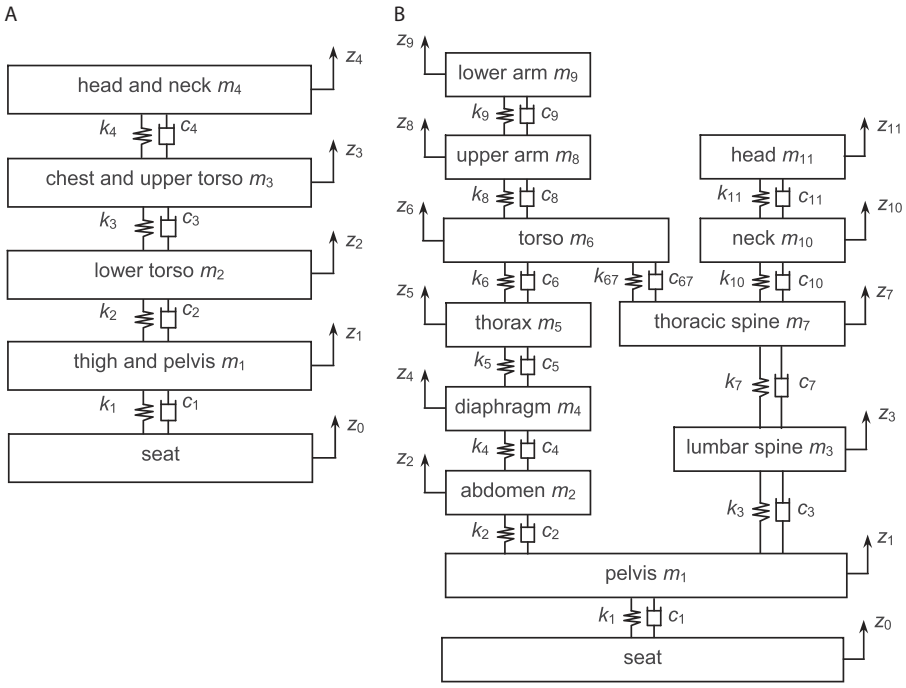

Figure 1. Biodynamic human body models analysed in the study: (a) Model 1 and (b) Model 2.
Note: c = coefficient of the damping elements; k = stiffness coefficient of the spring elements; m = mass of the related body segment; z = displacement of the related segment.

Table 1. Age and mass specifications of subjects.

Subject	Age (years)	Mass (kg)
S1	30	80.0
S2	21	78.0
S3	29	72.0
S4	20	76.5
S5	28	72.9
S6	20	84.3
S7	24	62.0
S8	27	77.7
S9	30	82.0
S10	20	79.0
M	24.9	76.4
SD	4.4	6.3

In order to record data, LMS SCADAS mobile data acquisition hardware (model SCM05; LMS International, Belgium) was used with LMS software Test.Lab version 12A. Two triaxial accelerometers (model T356A32; PCB Piezotronics, USA), one uniaxial accelerometer (model T333B32; PCB Piezotronics, USA) and one triaxial seat pad accelerometer (model 356B41; PCB Piezotronics, USA) were utilized for measurements. The two triaxial accelerometers and the uniaxial accelerometer were fixed onto the skin surface of the head, upper torso and lower torso of the subjects in order to measure the acceleration in a vertical direction. All accelerometers have a sensitivity of approximately 100 mV/g. Triaxial accelerometers can measure accelerations ranging from 1 to 4000 Hz. A uniaxial accelerometer can measure from 0.5 to 3000 Hz and a seat pad accelerometer can measure from 0.5 to 1000 Hz.

Approximate locations of the accelerometers, as well as the seating position of the subjects, are depicted in Figure 2. The accelerometers on the head, lower torso and upper torso were located on the middle side of the forehead, T3 vertebra and L3 vertebra, respectively. In order to keep the position of the accelerometers constant over the skin surface and to prevent slippage, adhesive tapes and flexible bandages were wrapped tightly around the corresponding body segment. Any probable disconnection between the skin surface and the accelerometer could be detected by the acceleration measurement system. A triaxial seat pad accelerometer was placed on the front-right seat in the vehicle fixed by means of self-adhesive tape. During the measurements, the subjects were asked to sit straight on the seat pad without having any contact with the backrest. In order to make sure the acceleration signals were recorded properly, all signals were investigated to observe whether there were any unexpected spikes within the signal content.

The head, upper torso and lower torso are common body components in the analysed models. Remaining body segments such as the viscera, neck, thoracic spine, lumbar spine, diaphragm, abdomen, etc., were not considered together in both models. Therefore measurement, calculation and evaluation processes were carried out for those three common segments, i.e., the head, upper torso and lower torso shown in Figure 2.

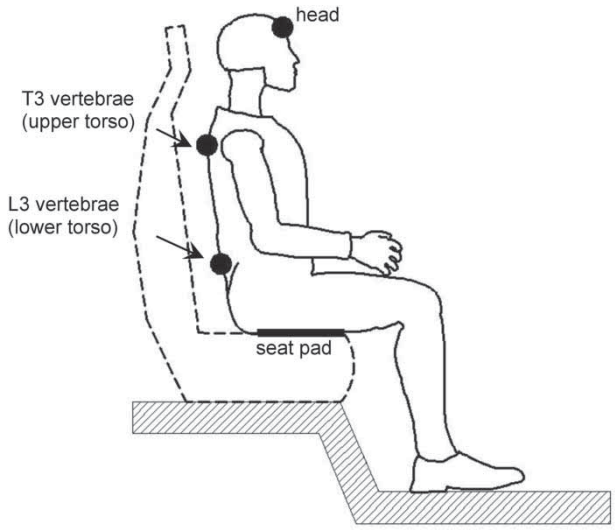

Figure 2. Positions of the accelerometers placed on subjects' bodies.

Equations of motion for the body models were obtained using Lagrangian principles and are presented in Appendix 2.

A large multipurpose vehicle was utilized for measurements. The subjects sat on the front seat and recording of vibration data was carried out by a technician who sat on the rear-left seat of the vehicle during the ride. Two types of asphalt pavements with different unevenness levels were selected for the car ride to be able to evaluate the effect of road surface quality and characteristics on the performances of biodynamic human body models. The first road was almost smooth and straight, while the unevenness level of the second road was remarkably high and straight. Hereafter the former will be referred to as Road I and the latter as Road II. For each road condition, two trials were carried out to eliminate possible inherent problems that can be stemmed from the experimental procedure. Thus, the total number of trials recorded during the experiments was 40 (10 subjects × 2 trials × 2 road types).

In the scope of measurements, acceleration data were collected for 30 s for each trial and the speed of the vehicle was fixed to 30 km/h during the ride. The sampling rate was 1600 Hz.

2.3. *Evaluation parameters*

Initially, each collected vertical acceleration data of the seat $\ddot{z}_0$ was post-processed in order to extract displacement (z_0) and velocity ($\dot{z}_0$) data as a function of time. Post-processing steps are demonstrated in Figure 3a and 3b. The raw acceleration data were first filtered by the sixth-order Butterworth high-pass filter with cut-off frequency of 1.33 Hz. Filtered data were then integrated using a cumulative trapezoidal method to obtain velocity data. The mean value of the integrated data was also subtracted by de-mean

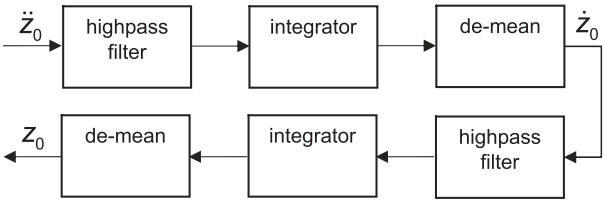

Figure 3. Post-processing steps to obtain velocity ($\dot{z}_0$) and displacement (z_0) from acceleration signal ($\ddot{z}_0$).
Note: z_0 = displacement of the seat pad; $\dot{z}_0$ = velocity of the seat pad; $\ddot{z}_0$ = acceleration of the seat pad.

operation. The same steps were applied to velocity data to reach displacement data of the seat afterwards. The displacement and velocity data of the seat were utilized as an input for human body models to generate motion response. By doing so, the same perturbation exposed to the human body was introduced into the models.

In order to sustain a quantified comparison between experimental and theoretical approaches, widely used vibration evaluation measures, i.e., rms acceleration for time-domain analysis and acceleration PSD for frequency domain analysis, were calculated.

In the study, acceleration data with 30-s time duration were scanned via a sliding and non-overlapped Hamming window. The width of the each segmented window was 1 s. Hence, after scanning of the whole acceleration data, 30 segments were obtained. The rms values of the acceleration data were calculated for each segmented window. The rms of the experimentally measured ($a_{\text{exp}}(t)$) and theoretically calculated ($a_{\text{the}}(t)$) accelerations with n samples was obtained from the following equation:

$$\text{rms} = \sqrt{\frac{\sum_n (x(n))^2}{n}}, \tag{1}$$

where rms = root mean square; $x(n)$ = acceleration data; n = number of samples.

PSD diagrams were estimated using Welch's method, which is an improved method of periodograms [45]. In Welch's method, data sets are segmented into overlapping or non-overlapping smaller pieces. Each piece of data is multiplied by a windowing function and their spectrums are then calculated and averaged in order to obtain the estimated PSD. In our case, 4096 data points for each segment with a Hamming window and 50% overlapping segments were used. The estimated PSD ($\hat{P}(f_n)$) of experimentally measured and theoretical calculated accelerations was obtained from the following equation:

$$\hat{P}(f_n) = \frac{1}{K\sum_{j=0}^{L-1} W^2(j)} \sum_{k=1}^{K} \left| \sum_{j=0}^{L-1} X_k(j) W(j) e^{-2kij f_n} \right|^2, \tag{2}$$

where $\hat{P}(f_n)$ = estimated power spectral density; L = length of segments; K = total number of segments;

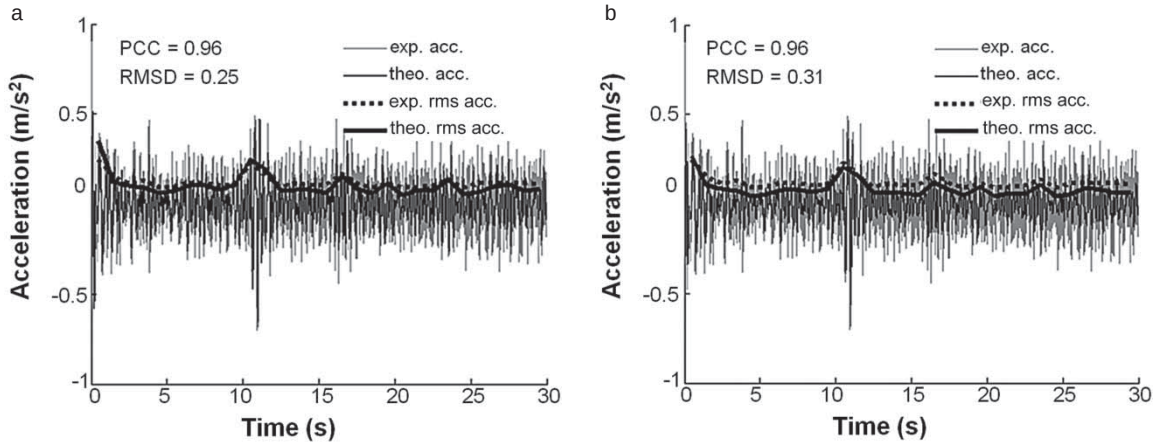

Figure 4. Representative demonstrations of the comparisons of the experimental and theoretical rms acceleration-time responses obtained from (a) Model 1 and (b) Model 2 for the lower torso during a ride on Road I.
Note: exp. acc. = time history of the experimental acceleration; exp. rms acc. = calculated root mean square values for each segmented window of time history of the experimental acceleration; PCC = Pearson correlation coefficient; RMSD = root mean square difference; theo. acc. = time history of the theoretical acceleration; theo. rms acc. = calculated root mean square values for each segmented window of time history of the theoretical acceleration.

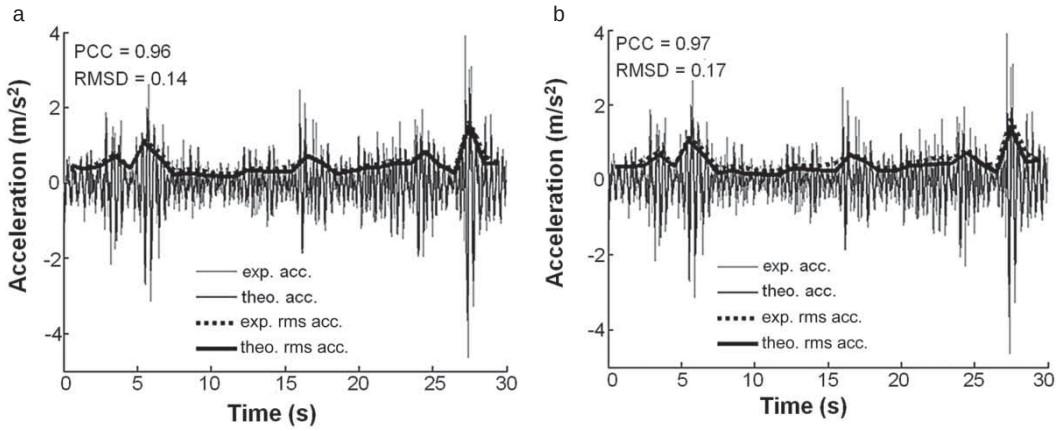

Figure 5. Representative demonstrations comparisons of the experimental and theoretical rms acceleration-time responses obtained from (a) Model 1 and (b) Model 2 for the lower torso during a ride on Road II.
Note: exp. acc. = time history of the experimental acceleration; exp. rms acc. = calculated root mean square values for each segmented window of time history of the experimental acceleration; PCC = Pearson correlation coefficient; RMSD = root mean square difference; theo. acc. = time history of the theoretical acceleration; theo. rms acc. = calculated root mean square values for each segmented window of time history of the theoretical acceleration.

$W(j)$ = related windowing function; $X_k(j)$ = kth segmented data; f_n = normalized frequency; i = imaginary unit; n = number of samples.

2.4. *Statistical and error analysis*

Simulation results provided by biodynamic models were assessed employing error and statistical analyses to quantify the unlabelled consequences of experimental and simulation works. Two parameters including the root mean square difference (RMSD) and the Pearson correlation coefficient (PCC) were considered to examine the accuracy and reliability of the findings. The RMSD between rms accelerations of experimental and theoretical cases can be obtained from the following equation:

$$\mathrm{RMSD} = \sqrt{\frac{\sum_{n=1}^{30} \left(\mathrm{rms}_{\mathrm{the}}(n) - \mathrm{rms}_{\mathrm{exp}}(n)\right)^2}{\sum \left(\mathrm{rms}_{\mathrm{exp}}(n)\right)^2}}, \qquad (3)$$

where RMSD = root mean square difference; $\mathrm{rms}_{\mathrm{the}}(n)$ = root mean square acceleration of theoretical accelerations; $\mathrm{rms}_{\mathrm{exp}}(n)$ = root mean square acceleration of experimental accelerations; n = number of samples.

Obtaining lower RMSD values means that high accuracy and closer acceleration results to the experimental cases in simulations are achieved by the proposed models. Accordingly, values that are close to 0 are sought in RMSD considerations since, e.g., a value of 0.01 RMSD represents

Table 2. RMSD values calculated between experimental and theoretical rms accelerations recorded on Road I.

	Head		Upper torso		Lower torso	
Subject	Model 1	Model 2	Model 1	Model 2	Model 1	Model 2
S1						
Trial 1	0.44	0.52	0.25	0.32	0.42	0.49
Trial 2	0.46	0.53	0.28	0.39	0.20	0.30
S2						
Trial 1	0.54	0.62	0.21	0.30	0.32	0.40
Trial 2	0.24	0.45	0.10	0.37	0.19	0.38
S3						
Trial 1	0.43	0.51	0.23	0.26	0.19	0.31
Trial 2	0.36	0.45	0.21	0.28	0.18	0.28
S4						
Trial 1	0.45	0.48	0.42	0.30	0.53	0.44
Trial 2	0.35	0.43	0.26	0.31	0.37	0.34
S5						
Trial 1	0.33	0.46	n/a[a]	n/a[a]	0.27	0.37
Trial 2	0.37	0.40	n/a[a]	n/a[a]	0.26	0.38
S6						
Trial 1	0.39	0.50	0.32	0.31	0.21	0.36
Trial 2	0.34	0.50	0.23	0.24	0.23	0.39
S7						
Trial 1	0.31	0.40	0.14	0.27	0.15	0.25
Trial 2	0.33	0.42	0.15	0.31	0.17	0.27
S8						
Trial 1	0.46	0.17	0.39	0.16	0.19	0.21
Trial 2	0.26	0.33	0.19	0.32	0.29	0.42
S9						
Trial 1	0.52	0.53	0.36	0.23	0.13	0.23
Trial 2	0.27	0.31	0.68	0.23	0.17	0.19
S10						
Trial 1	0.34	0.39	0.23	0.34	0.25	0.31
Trial 2	0.30	0.39	0.20	0.30	0.18	0.33
M	0.37	0.44	0.27	0.29	0.25	0.33
SD	0.08	0.10	0.13	0.05	0.10	0.08

[a]A problem occurred with the contact interface between the accelerometer attached on the upper torso and the skin surface, which was noticed after completion of the experiments. Therefore, no experimental data are available for the upper torso of Subject 5.
Note: n/a = not available; rms = root mean square; RMSD = root mean square difference.

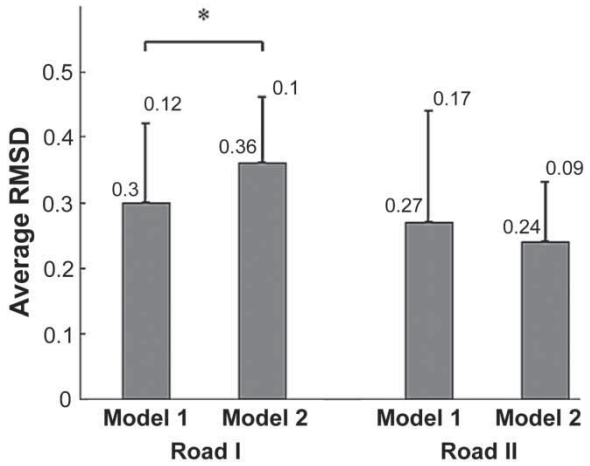

Figure 6. Overall mean values of RMSD between experimental and simulation rms accelerations obtained by taking all body segments and trials into account.
*$p < 0.05$
Note: Error bars denote *SD* of mean RMSD values.
RMSD = root mean square difference.

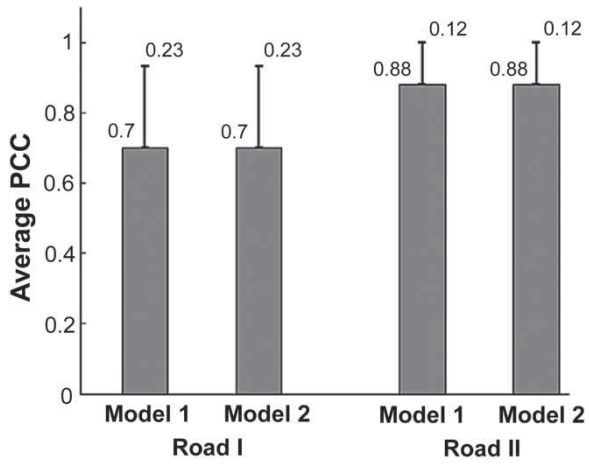

Figure 7. Overall mean values of PCC between experimental and simulation rms accelerations obtained by taking all body segments and trials into account.
Note: Error bars denote *SD* of mean PCC values.
PCC = Pearson correlation coefficient.

Table 3. RMSD values calculated between experimental and theoretical rms accelerations recorded on Road II.

	Head		Upper torso		Lower torso	
Subject	Model 1	Model 2	Model 1	Model 2	Model 1	Model 2
S1						
Trial 1	0.32	0.33	0.24	0.21	0.13	0.14
Trial 2	0.97	0.39	0.23	0.20	0.11	0.14
S2						
Trial 1	0.24	0.29	0.12	0.23	0.20	0.26
Trial 2	0.25	0.30	0.10	0.22	0.20	0.26
S3						
Trial 1	0.34	0.34	0.21	0.18	0.08	0.14
Trial 2	0.40	0.42	0.17	0.14	0.08	0.13
S4						
Trial 1	0.49	0.40	0.43	0.26	0.11	0.15
Trial 2	0.32	0.36	0.55	0.34	0.13	0.17
S5						
Trial 1	0.30	0.26	n/a[a]	n/a[a]	0.16	0.20
Trial 2	0.52	0.46	n/a[a]	n/a[a]	0.23	0.26
S6						
Trial 1	0.54	0.41	0.27	0.16	0.10	0.17
Trial 2	0.32	0.26	0.25	0.16	0.16	0.22
S7						
Trial 1	0.43	0.34	0.08	0.14	0.07	0.12
Trial 2	0.51	0.44	0.11	0.14	0.10	0.13
S8						
Trial 1	0.52	0.36	0.24	0.15	0.09	0.14
Trial 2	0.44	0.30	0.28	0.17	0.12	0.15
S9						
Trial 1	0.50	0.40	0.31	0.19	0.08	0.10
Trial 2	0.40	0.37	0.28	0.16	0.07	0.11
S10						
Trial 1	0.41	0.28	0.22	0.19	0.14	0.17
Trial 2	0.41	0.32	0.25	0.22	0.12	0.18
M	0.43	0.35	0.24	0.19	0.12	0.17
SD	0.16	0.06	0.11	0.05	0.05	0.05

[a]A problem occurred with the contact interface between the accelerometer attached on the upper torso and the skin surface, which was noticed after completion of the experiments. Therefore, no experimental data are available for the upper torso of Subject 5.
Note: n/a = not available; rms = root mean square; RMSD = root mean square difference.

1% mean error from experimental acceleration measurements. In addition, PCC values between rms accelerations, as well as between acceleration PSDs, of experimental and theoretical cases were calculated to measure the similarity of traces and to determine which model provides the most representative and realistic results. The PCC was expressed as follows:

$$\mathrm{PCC} = \frac{C_{\mathrm{et}}(0)}{\sqrt{C_{\mathrm{tt}}(0)}\sqrt{C_{\mathrm{ee}}(0)}}, \tag{4}$$

where PCC = Pearson correlation coefficient; $C_{\mathrm{et}}(0)$ = covariance of $a_{\mathrm{exp}}(t)$ and $a_{\mathrm{the}}(t)$; $C_{\mathrm{tt}}(0)$ = autovariance of $a_{\mathrm{the}}(t)$; $C_{\mathrm{ee}}(0)$ = autovariance of $a_{\mathrm{exp}}(t)$; $a_{\mathrm{exp}}(t)$ = experimentally measured acceleration; $a_{\mathrm{the}}(t)$ = theoretically calculated acceleration.

The PCC implies similarity between two data sets. For example, if the PCC value between two data sets is found to be 1, this means that these two sets are completely equivalent, while 0 represents totally non-equivalent. Moreover, one-way analysis of variance (ANOVA) was performed to examine the significance of differences between the results obtained from Model 1 and Model 2. In order to carry out the analysis, the mean and *SD* of rms accelerations and acceleration PSD were calculated and then compared from a statistical point of view. The level of significance was set at 0.05 ($p < 0.05$).

3. Results

For a quantitative time domain evaluation, the RMSD and PCC were calculated between experimentally and theoretically obtained acceleration rms results. Typical comparisons of rms accelerations, which were obtained from Model 1 and Model 2, with the experimentally obtained value for the lower torso (Subject S10, Trial 1) are presented in Figure 4 for Road I and Figure 5 for Road II. The calculated RMSD and PCC values between the respective experimental and theoretical rms accelerations are also shown in the figures. It can be observed from Figures 4

Table 4. PCC values calculated between experimental and theoretical rms accelerations recorded on Road I.

	Head		Upper torso		Lower torso	
Subject	Model 1	Model 2	Model 1	Model 2	Model 1	Model 2
S1						
Trial 1	0.54	0.51	0.90	0.91	0.89	0.89
Trial 2	0.14	0.16	0.68	0.72	0.90	0.92
S2						
Trial 1	0.49	0.46	0.94	0.92	0.92	0.92
Trial 2	0.63	0.62	0.93	0.90	0.97	0.94
S3						
Trial 1	0.40	0.48	0.90	0.92	0.96	0.96
Trial 2	0.54	0.55	0.83	0.83	0.91	0.89
S4						
Trial 1	0.27	0.29	0.73	0.74	0.36	0.34
Trial 2	0.59	0.61	0.73	0.71	0.54	0.54
S5						
Trial 1	0.09	0.01	n/a	n/a	0.52	0.51
Trial 2	0.24	0.24	n/a	n/a	0.49	0.49
S6						
Trial 1	0.39	0.40	0.76	0.79	0.96	0.93
Trial 2	0.60	0.65	0.87	0.90	0.92	0.91
S7						
Trial 1	0.51	0.42	0.91	0.90	0.93	0.93
Trial 2	0.55	0.48	0.93	0.92	0.96	0.96
S8						
Trial 1	0.74	0.80	0.82	0.85	0.76	0.79
Trial 2	0.58	0.62	0.76	0.75	0.74	0.77
S9						
Trial 1	0.30	0.43	0.68	0.73	0.85	0.77
Trial 2	0.59	0.63	0.79	0.82	0.87	0.84
S10						
Trial 1	0.80	0.79	0.93	0.92	0.96	0.96
Trial 2	0.37	0.34	0.81	0.82	0.90	0.89
M	0.47	0.47	0.83	0.84	0.82	0.81
SD	0.19	0.20	0.09	0.08	0.19	0.19

Note: PCC = Pearson correlation coefficient; rms = root mean square.

and 5 that the amplitudes of the accelerations recorded under the Road II conditions are higher than those recorded under the Road I conditions, which is an expected outcome because Road II was rougher than Road I.

RMSD values calculated between experimental and theoretical rms accelerations obtained for each trial under the Road I conditions are presented in Table 2 and those under the Road II conditions in Table 3. In the tables, the mean and *SD* of rms accelerations are also presented. Under the Road I conditions, the mean RMSD results were obtained as 0.37, 0.27 and 0.25 from Model 1 and 0.44, 0.29 and 0.33 from Model 2 for the head, upper torso and lower torso, respectively (Table 2). According to the mean rms acceleration results, lower RMSD values were obtained using Model 1 than those from Model 2 for all body segments under the Road I conditions, which indicates that Model 1 showed better characterizing performance than Model 2 with respect to the error rate in the representation of the experimental acceleration amplitude.

Under the Road II conditions, the mean RMSD results were obtained as 0.43, 0.24 and 0.12 from Model 1 and 0.35, 0.19 and 0.17 from Model 2 for the head, upper torso and lower torso, respectively (Table 3). According to the mean rms acceleration results, lower RMSD values were obtained using Model 2 than those from Model 1 for the head and upper torso segments, but a better result was obtained from Model 1 than that from Model 2 for the lower torso under the Road II conditions.

The overall mean RMSD results between experimental and simulation rms accelerations were calculated by averaging all RMSD values obtained for each trial of all body segments for each human body model, and are shown in Figure 6. It can be deduced from the figure that Model 1 outperformed Model 2 in characterizing the real human body behaviour under the Road I conditions ($p = 0.004$); on the other hand, Model 2 gave a lower overall mean value of RMSD under the Road II conditions ($p = 0.286$).

PCC values calculated between experimental and theoretical rms accelerations obtained for each trial under the Road I conditions are presented in Table 4 and under the Road II conditions in Table 5. Under the Road I conditions,

Table 5. PCC values calculated between experimental and theoretical rms accelerations recorded on Road II.

	Head		Upper torso		Lower torso	
Subject	Model 1	Model 2	Model 1	Model 2	Model 1	Model 2
S1						
Trial 1	0.79	0.80	0.92	0.92	0.98	0.97
Trial 2	0.62	0.63	0.92	0.92	0.97	0.97
S2						
Trial 1	0.84	0.85	0.97	0.97	0.98	0.97
Trial 2	0.81	0.81	0.98	0.98	0.98	0.98
S3						
Trial 1	0.69	0.68	0.93	0.93	0.98	0.98
Trial 2	0.56	0.54	0.97	0.97	0.99	0.98
S4						
Trial 1	0.53	0.60	0.89	0.91	0.80	0.79
Trial 2	0.75	0.73	0.92	0.91	0.82	0.81
S5						
Trial 1	0.86	0.85	n/a	n/a	0.95	0.94
Trial 2	0.43	0.45	n/a	n/a	0.90	0.88
S6						
Trial 1	0.75	0.72	0.97	0.96	0.99	0.99
Trial 2	0.92	0.92	0.98	0.97	0.99	0.98
S7						
Trial 1	0.85	0.86	0.99	0.97	0.99	0.97
Trial 2	0.82	0.82	0.99	0.98	0.99	0.99
S8						
Trial 1	0.91	0.91	0.98	0.97	0.99	0.98
Trial 2	0.89	0.88	0.95	0.95	0.98	0.97
S9						
Trial 1	0.69	0.67	0.95	0.95	0.99	0.99
Trial 2	0.70	0.70	0.86	0.96	0.99	0.99
S10						
Trial 1	0.86	0.89	0.93	0.94	0.96	0.97
Trial 2	0.81	0.78	0.91	0.89	0.97	0.96
M	0.75	0.75	0.95	0.95	0.96	0.95
SD	0.13	0.13	0.04	0.03	0.06	0.06

Note: PCC = Pearson correlation coefficient; rms = root mean square.

the mean PCC results were obtained as 0.47, 0.83 and 0.82 from Model 1 and 0.47, 0.84 and 0.81 from Model 2 for the head, upper torso and lower torso, respectively (Table 4). Under the Road II conditions, the mean PCC results were obtained as 0.75, 0.95 and 0.96 from Model 1 and 0.75, 0.95 and 0.95 from Model 2 for the head, upper torso and lower torso, respectively (Table 5). According to the mean PCC values obtained between experimental and theoretical rms acceleration results, Model 1 and Model 2 demonstrated similar performance in imitating the human body response under WBV.

The overall mean PCC results between experimental and simulation rms accelerations were calculated by averaging all PCC values obtained for each trial of all body segments for each human body model, and are shown in Figure 7. It can be deduced from the mean results that Model 1 and Model 2 showed nearly equivalent response under vibration in terms of the PCC evaluation.

For a quantitative frequency domain evaluation, PCC values were calculated between experimentally and theoretically obtained acceleration PSD results. Typical comparisons of acceleration PSDs, which were obtained from Model 1 and Model 2, with the experimentally obtained value for the lower torso (Subject S10, Trial 1) are presented in Figure 8 for Road I and Figure 9 for Road II. The calculated PCC values between the respective experimental and theoretical acceleration PSD values are also shown in the figures. The same effect of road roughness can be observed on the magnitude of the acceleration PSD data as seen in the acceleration-time histories (Figures 4 and 5), in such a way that the acceleration PSD magnitudes obtained under the Road II conditions are higher than those recorded under the Road I conditions.

PCC values calculated between experimental and theoretical acceleration PSDs obtained for each trial under the Road I conditions are presented in Table 6 and under the Road II conditions in Table 7. Under the Road I conditions, the mean PCC results were obtained as 0.71, 0.84 and 0.90 from Model 1 and 0.79, 0.88 and 0.90 from Model 2 for the head, upper torso and lower torso, respectively (Table 6). Higher PCC values were obtained using Model 2 than those from Model 1 for the head and upper torso, and an

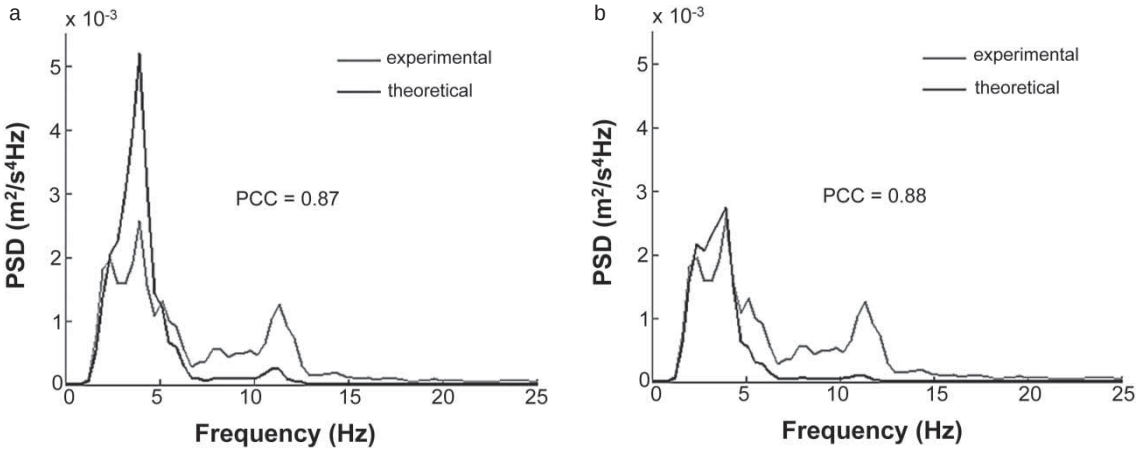

Figure 8. Representative demonstrations of the comparisons of the experimental and theoretical acceleration PSDs obtained from (a) Model 1 and (b) Model 2 for the lower torso during a ride on Road I.
Note: PCC = Pearson correlation coefficient; PSD = power spectral density.

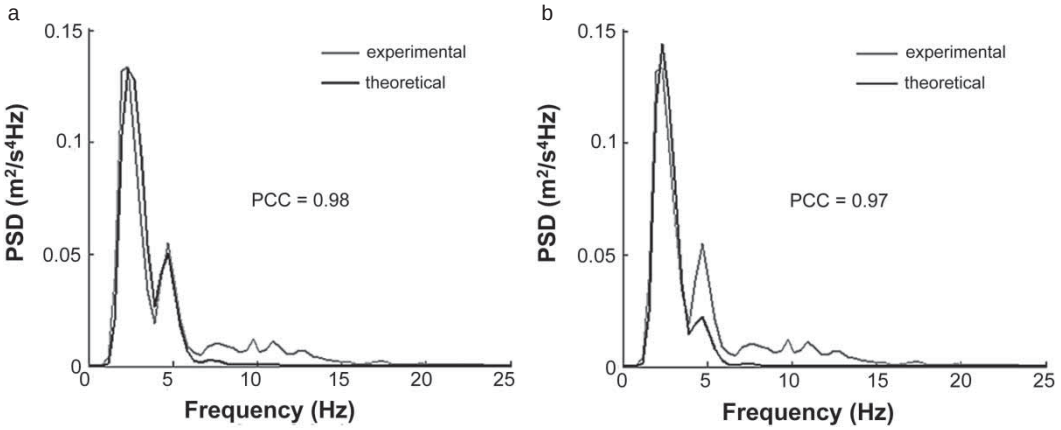

Figure 9. Representative demonstrations of the comparisons of the experimental and theoretical acceleration PSDs obtained from (a) Model 1 and (b) Model 2 for the lower torso during a ride on Road II.
Note: PCC = Pearson correlation coefficient; PSD = power spectral density.

equivalent mean value was obtained from both models for the lower torso under the Road I conditions.

The overall mean PCC results between experimental and simulation acceleration PSD values were calculated by averaging all PCC values obtained for each trial of all body segments for each human body model, and are shown in Figure 10. Model 2 provided higher PCC results than Model 1 for the Road I ($p = 0.112$) and Road II ($p = 0.275$) conditions. These findings indicate that Model 2 showed better characterizing performance of the real human body behaviour than Model 1 in terms of the frequency content of the acceleration. Significant difference was not found between the PCC values of Model 1 and Model 2.

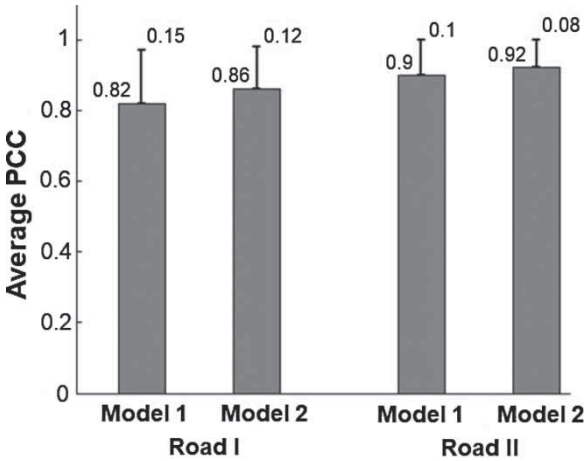

Figure 10. Overall mean values of PCC between experimental and simulation acceleration PSDs obtained by taking all body segments and trials into account.
Note: Error bars denote *SD* of mean PCC values.
PCC = Pearson correlation coefficient.

4. Discussion

There are different types of human body models, such as lumped-parameter, finite element and multibody models that are aimed to characterize the human body behaviours

Table 6. PCC values calculated between experimental and theoretical acceleration PSD values recorded on Road I.

	Head		Upper torso		Lower torso	
Subject	Model 1	Model 2	Model 1	Model 2	Model 1	Model 2
S1						
Trial 1	0.83	0.92	0.83	0.91	0.86	0.93
Trial 2	0.78	0.9	0.84	0.93	0.96	0.97
S2						
Trial 1	0.57	0.68	0.92	0.93	0.94	0.92
Trial 2	0.82	0.88	0.99	0.96	0.99	0.97
S3						
Trial 1	0.81	0.83	0.52	0.89	0.93	0.91
Trial 2	0.81	0.86	0.79	0.84	0.89	0.86
S4						
Trial 1	0.71	0.86	0.75	0.72	0.90	0.9
Trial 2	0.91	0.95	0.93	0.93	0.44	0.45
S5						
Trial 1	0.87	0.91	n/a	n/a	0.86	0.92
Trial 2	0.52	0.58	n/a	n/a	0.95	0.96
S6						
Trial 1	0.55	0.68	0.89	0.92	0.98	0.94
Trial 2	0.49	0.58	0.93	0.93	0.96	0.94
S7						
Trial 1	0.76	0.86	0.95	0.92	0.97	0.96
Trial 2	0.84	0.84	0.95	0.94	0.95	0.95
S8						
Trial 1	0.76	0.82	0.98	0.98	0.98	0.98
Trial 2	0.68	0.76	0.75	0.74	0.69	0.68
S9						
Trial 1	0.42	0.56	0.94	0.96	0.98	0.98
Trial 2	0.84	0.91	0.77	0.84	0.95	0.98
S10						
Trial 1	0.66	0.79	0.65	0.69	0.87	0.88
Trial 2	0.60	0.72	0.82	0.86	0.95	0.95
M	0.71	0.79	0.84	0.88	0.90	0.90
SD	0.14	0.12	0.12	0.09	0.13	0.13

Note: PCC = Pearson correlation coefficient; PSD = power spectral density.

in cases of executing some motion patterns, exposing environmental disturbances or designing ergonomic occupational equipments [25]. Lumped-parameter models are comprised of concentrated masses interconnected by rheological elements, namely spring and dashpots that enable the kinematic and kinetic analysis of the human body to be carried out. Unlike the lumped-parameter type, finite element models follow a continuum-mechanical modelling approach in which stress and strain analysis can be done over the biological tissues. Multibody human body models consist of rigid links interconnected by joints which constrain the movement of one link to another. Multibody models are quite convenient for kinematic and kinetic simulations of the human body. Compared to the finite element and multibody models, lumped-parameter models are easier to analyse, more flexible to be adapted to different physical conditions and more eligible to validate with experiments. One of the main disadvantages of such models is the limitation to one-directional analysis [25].

Lumped-parameter human body models are supposed to present basic biodynamic behaviours of living bodies under WBV. The use of such models has the potential to allow the prediction of the drivers' vibration exposure levels and the seat's ability to reduce vibration in vehicles. Since the vibration measurement from the human body is expensive and includes safety and health risk concerns, reliable physical models that are capable of imitating the response of the real human body can be used as a convenient tool in evaluation of the effects of the destructive vibration exposures.

In the study, two different rheological human body models were investigated with respect to the time (rms acceleration) and frequency (acceleration PSD) responses under dynamic conditions. When the RMSD results of the rms accelerations are taken into account it can be concluded that Model 1 showed better characterizing performance than Model 2 under the Road I conditions ($p < 0.05$). However, for the Road II riding case, Model 2 provided lower RMSD mean value than Model 1

Table 7. PCC values calculated between experimental and theoretical acceleration PSD values recorded on Road II.

	Head		Upper torso		Lower torso	
Subject	Model 1	Model 2	Model 1	Model 2	Model 1	Model 2
S1						
Trial 1	0.97	0.96	0.92	0.97	0.99	0.99
Trial 2	0.86	0.91	0.87	0.94	0.97	0.99
S2						
Trial 1	0.89	0.94	0.98	0.98	0.99	0.99
Trial 2	0.89	0.91	0.98	0.98	0.99	0.98
S3						
Trial 1	0.91	0.93	0.96	0.98	0.99	0.97
Trial 2	0.57	0.65	0.97	0.98	0.99	0.98
S4						
Trial 1	0.79	0.85	0.86	0.88	0.73	0.71
Trial 2	0.82	0.90	0.93	0.94	0.94	0.93
S5						
Trial 1	0.91	0.96	n/a	n/a	0.96	0.98
Trial 2	0.61	0.70	n/a	n/a	0.95	0.98
S6						
Trial 1	0.83	0.88	0.94	0.97	1	0.99
Trial 2	0.87	0.89	0.95	0.97	1	0.99
S7						
Trial 1	0.85	0.90	0.97	0.97	0.99	0.99
Trial 2	0.77	0.82	0.99	0.98	1	0.99
S8						
Trial 1	0.88	0.90	0.95	0.95	0.99	0.97
Trial 2	0.83	0.88	0.94	0.96	0.98	0.98
S9						
Trial 1	0.78	0.82	0.90	0.95	0.99	0.99
Trial 2	0.51	0.58	0.89	0.92	0.99	0.99
S10						
Trial 1	0.87	0.86	0.89	0.88	0.98	0.97
Trial 2	0.75	0.79	0.83	0.86	0.97	0.98
M	0.81	0.85	0.93	0.95	0.97	0.97
SD	0.12	0.10	0.05	0.04	0.06	0.06

Note: PCC = Pearson correlation coefficient; PSD = power spectral density.

($p > 0.05$). In terms of the PCC evaluation of rms accelerations, it was observed that Model 1 and Model 2 responded equivalently under WBV (Figure 7). In the PCC analysis of the frequency content of the acceleration signals it was found that Model 2 showed higher agreement with the experimental data, thereby indicating that Model 2 showed more similar strength and direction of association to the experimental data than Model 1. However, no significant difference was found between PCC values of the models.

Liang and Chiang [24] analysed some lumped-parameter models, which were exposed to vertical vibration, from the literature in terms of seat-to-head transmissibility, driving-point mechanical impedance and apparent mass. They synthesized various experimental data from published literature to evaluate the models. They evaluated the models by taking into account the ratio of the rms error to the mean value calculated for seat-to-head transmissibility, driving-point mechanical impedance and apparent mass. Although the results were not analysed statistically, it can be deduced from the study that the characterization performances of the biodynamic models varied according to the evaluation criterion, which is consistent with the results of our study as Model I and Model II showed different prediction capability according to the time and frequency contents. Moreover, we showed in our study that the road conditions also affected the prediction performance of the theoretical models, thereby indicating that further modelling studies are needed to obtain more accurate and robust simulation results.

One of the limitations of this study is that only a small number of models was evaluated. This choice was made in order to analyse these two widely used models in detail. These two models are not of interest for the vibration exposure in horizontal directions. Therefore, in addition to the vibrations in the vertical direction, investigation of the adverse effects of the horizontal vibrations would also contribute valuable information to the research community. In order to assess the effect of vehicle speed on the characterizing performance of the models, different speed levels could also be tested in the experiments, which we did not do in this study so as to prevent any unintended health risk to the subjects.

5. Conclusion

By taking all of the time and frequency response results into account it can be concluded that neither of the models showed the best prediction performance of human body behaviour in all of the cases. Model 1 outperformed Model 2 in representing real human body behaviour during a vehicle ride on a smooth road surface. However, Model 2 provided better agreement with the experimental data than Model 1 for the vehicle ride on a rough surface. There still needs to be further investigation conducted to reach improved physical models that are capable of better predicting human body responses under WBV. Parameter identification studies for different excitation and road conditions including a large number of human subjects would provide more reliable models than the existing ones. It is expected that the outcomes of the study would contribute to the use of biodynamic models in better understanding vibration effects on the human body.

Disclosure statement

No potential conflict of interest was reported by the authors.

ORCID

Yunus Ziya Arslan http://orcid.org/0000-0002-1861-9368

References

[1] Blüthner R, Seidel H, Hinz B. Myoelectric response of back muscles to vertical random whole-body vibration with different magnitudes at different postures. J Sound Vib. 2002;253(1):37–56. doi:10.1006/jsvi.2001.4248

[2] Griffin MJ. Discomfort from feeling vehicle vibration. Vehicle Syst Dyn. 2007;45(7):679–698. doi:10.1080/00423110701422426

[3] Balandin DV, Bolotnik NN, Pilkey WD. Optimal protection from impact, shock and vibration. Amsterdam: Gordon and Breach Science; 2001.

[4] Seidel H. Selected health risks caused by long-term, whole-body vibration. Am J Ind Med. 1993;23:589–604. doi:10.1002/ajim.4700230407

[5] Hulshof C, van Zanten BV. Whole-body vibration and low-back pain. Int Arch Occup Environ Health. 1987;59:205–220. doi:10.1007/BF00377733

[6] Miyashita K, Morioka I, Tanabe T, et al. Symptoms of construction workers exposed to whole body vibration and local vibration. Int Arch Occup Environ Health. 1992;64:347–351. doi:10.1007/BF00379545

[7] Bonney RA. Human responses to vibration: principles and methods. In: Wilson JR, Corlett EN, editors. Evaluation of human work: a practical ergonomics methodology. Philadelphia (PA): Taylor & Francis; 1999. p. 541–556.

[8] Arslan YZ. Experimental assessment of lumped-parameter human body models exposed to whole body vibration. J Mech Med Biol. 2015;15:1550023. doi:10.1142/S0219519415500232

[9] Mani R, Milosavljevic S, Sullivan SJ. The effect of occupational whole-body vibration on standing balance: a systematic review. Int J Ind Ergon. 2010;40(6):698–709. doi:10.1016/j.ergon.2010.05.009

[10] Zahov V, Medzhidieva D. Vestibular disturbances in operators of over-ground machinery in Bobov Dol coal mines. Acta Medica Bulgarica. 2005;32:68–71.

[11] Huxham FE, Goldie PA, Patla AE. Theoretical considerations in balance assessment. Aust J Physiother. 2001;47:89–100. doi:10.1016/S0004-9514(14)60300-7

[12] Ng JK, Parnianpour M, Richardson CA, et al. Effect of fatigue on torque output and electromyographic measures of trunk muscles during isometric axial rotation. Arch Phys Med Rehabil. 2003;84:374–381. doi:10.1053/apmr.2003.50008

[13] Santos, BR, Lariviere C, Delisle A, et al. A laboratory study to quantify the biomechanical responses to whole-body vibration: the influence on balance, reflex response, muscular activity and fatigue. Int J Ind Ergon. 2008;38:626–639. doi:10.1016/j.ergon.2008.01.015

[14] Bovenzi M, Hulshof CTJ. An updated review of epidemiologic studies on the relationship between exposure to whole-body vibration and low back pain. J Sound Vib. 1998;215:595–611. doi:10.1006/jsvi.1998.1598

[15] Cornelius KM, Redfern MS, Steiner LJ. Postural stability after whole-body vibration exposure. Int J Ind Ergon. 1994;13:343–351. doi:10.1016/0169-8141(94)90091-4

[16] Lings S, Leboeuf-Yde C. Whole-body vibration and low back pain: a systematic, critical review of the epidemiological literature 1992–1999. Int Arch Occup Environ Health. 2000;73:290–297. doi:10.1007/s004200000118

[17] Griffin MJ. A comparison of standardized methods for predicting the hazards of whole-body vibration and repeated shocks. J Sound Vib. 1998;215:883–914. doi:10.1006/jsvi.1998.1600

[18] Beard GF, Griffin MJ. Discomfort during lateral acceleration: influence of seat cushion and backrest. Appl Ergon. 2013;44(4):588–594. doi:10.1016/j.apergo.2012.11.009

[19] Ebe K, Griffin MJ. Quantitative prediction of overall seat discomfort. Ergonomics. 2000;43(6):791–806. doi:10.1080/001401300404751

[20] Liang CC, Chiang CF, Nguyen TG. Biodynamic responses of seated pregnant subjects exposed to vertical vibrations in driving conditions. Vehicle Syst Dyn. 2007;45:1017–1049. doi:10.1080/00423110601176668

[21] Holmlund P, Lundstrom R. Mechanical impedance of the human body in the horizontal direction. J Sound Vib. 1998;215(4):801–812. doi:10.1006/jsvi.1998.1593

[22] Rehn B, Nilsson T, Olofsson B, et al. Whole-body vibration exposure and non-neutral neck postures during occupational use of all-terrain vehicles. Ann Occup Hyg. 2005;49:267–275.

[23] Chen JC, Chang WR, Chang W, et al. Occupational factors associated with low back pain in urban taxi drivers. Occup Med (Lond). 2005;55:535–540. doi:10.1093/occmed/kqi125

[24] Liang CC, Chiang CF. A study on biodynamic models of seated human subjects exposed to vertical vibration. Int J Ind Ergon. 2006;36:869–890. doi:10.1016/j.ergon.2006.06.008

[25] Fairley TE, Griffin MJ. The apparent mass of the seated human body in the fore-and-aft and lateral directions. J Sound Vib. 1990;139:299–306. doi:10.1016/0022-460X(90)90890-C

[26] Fritz M. Dynamic properties of the biomechanical model of the human body – influence of posture and direction of vibration stress. J Low Freq Noise Vib Active Contr. 2005;24(4):233–249. doi:10.1260/026309205776232808

[27] Boileau PÉ, Rakheja S. Whole-body vertical biodynamic response characteristics of the seated vehicle driver:

measurement and model development. Int J Ind Ergon. 1998;22:449–472. doi:10.1016/S0169-8141(97)00030-9
[28] Magnusson M, Pope M, Rosredt M, et al. Effect of backrest inclination on the transmission of vertical vibrations through the lumbar spine. Clin Biomech (Bristol, Avon). 1993;8:5–12. doi:10.1016/S0268-0033(05)80003-8
[29] Muksian R, Nash CD. A model for the response of seated humans to sinusoidal displacements of the seat. J Biomech. 1974;7:209–215. doi:10.1016/0021-9290(74)90011-6
[30] Muksian R, Nash CD. On frequency-dependent damping coefficients in lumped-parameter models of human beings. J Biomech. 1976;9:339–342. doi:10.1016/0021-9290(76)90055-5
[31] Patil MK, Palanichamy MS, Ghista DN. Man–tractor system dynamics: towards a better suspension system for human ride comfort. J Biomech. 1978;11:397–406. doi:10.1016/0021-9290(78)90074-X
[32] Qassem W, Othman MO, Abdul-Majeed S. The effects of vertical and horizontal vibrations on the human body. Med Eng Phys. 1994;16:151–161. doi:10.1016/1350-4533(94)90028-0
[33] Qassem W. Model prediction of vibration effects on human subject seated on various cushions. Med Eng Phys. 1996;18(5):350–358. doi:10.1016/1350-4533(95)00060-7
[34] Wan Y, Schimmels JM. A simple model that captures the essential dynamics of a seated human exposed to whole body vibration. Adv Bioeng. 1995;31:333–334.
[35] Mertens H. Nonlinear behavior of sitting humans under increasing gravity. Aviat Space Environ Med. 1978;49(1):287–298.
[36] Kim SK, White SW, Bajaj AK, et al. Simplified models of the vibration of mannequins in car seats. J Sound Vib. 2003;264(1):49–90. doi:10.1016/S0022-460X(02)01164-1
[37] Wei L, Griffin J. The prediction of seat transmissibility from measures of seat impedance. J Sound Vib. 1998;214(1):121–137. doi:10.1006/jsvi.1998.1540
[38] Zhao Y, Zhao L, Gao H. Vibration control of seat suspension using H∞ reliable control. J Vib Control. 2010;16(12):1859–1879. doi:10.1177/1077546309349852
[39] Abdeen MAM, Abbas W. Prediction the biodynamic response of the seated human body using artificial intelligence technique. Int J Eng. 2011;4:463–506.
[40] Srdjevic Z, Cveticanin L. Entropy compromise programming method for parameter identification in the seated driver biomechanical model. Int J Ind Ergon. 2004;34(4):307–318. doi:10.1016/j.ergon.2004.04.010
[41] Linan X, Mingli L, Xiaochun S, et al. Human vibration characteristic and experiment research on man–machine system in dynamic environment. Paper presented at: 9th International Conference on Computer-Aided Industrial Design and Conceptual Design; 2002 Nov 22–25; Kunming, China.
[42] Jarrah M, Qassem W, Othman M, et al. Human body model response to mechanical impulse. Med Eng Phys. 1997;19:308–316. doi:10.1016/S1350-4533(96)00081-1
[43] Qassem W, Jarrah M, Othman M. Heart response to horizontal impulse. J Med Eng Technol. 1998;22:82–90. doi:10.3109/03091909809010003
[44] International Organization for Standardization (ISO). Mechanical vibration and shock – guidance on safety aspects of tests and experiments with people, Part 1: exposure to whole-body mechanical vibration and repeated shock. Geneva: ISO; 1998. Standard No. ISO 13090–1:1998.
[45] Welch PD. The use of fast Fourier transform for the estimation of power spectra: a method based on time averaging over short, modified periodograms. IEEE Trans Audio Electroacoust. 1967;15:70–73. doi:10.1109/TAU.1967.1161901

Appendix 1

Table A.1. Numerical values of the parameters of Model 1.

Mass (kg)	Stiffness (N/m)	Damping (N·s/m)
m_1: 12.733	k_1: 90,000	c_1: 2064
m_2: 8.588	k_2: 162,800	c_2: 4548
m_3: 28.386	k_3: 183,000	c_3: 4750
m_4: 5.290	k_4: 310,000	c_4: 400

Note: c = coefficient of the damping elements; k = stiffness coefficient of the spring elements; m = mass of the related body segments.

Table A.2. Numerical values of the parameters of Model 2.

Mass (kg)	Stiffness (N/m)	Damping (N·s/m)
m_1: 16.332	k_1: 25,016	c_1: 370.8
m_2: 3.542	k_2: 877	c_2: 292.3
m_3: 1.200	k_3: 52,621	c_3: 3581.6
m_4: 0.272	k_4: 877	c_4: 292.3
m_5: 0.816	k_5: 877	c_5: 292.3
m_6: 19.611	k_6: 52,621	c_6: 3581.6
m_7: 2.882	k_{67}: 877	c_{67}: 292.3
m_8: 3.280	k_7: 52,621	c_7: 3581.6
m_9: 3.177	k_8: 67,542	c_8: 3581.6
m_{10}: 0.650	k_9: 67,542	c_9: 3581.6
m_{11}: 3.265	k_{10}: 52,621	c_{10}: 3581.6
–	k_{11}: 52,621	c_{11}: 3581.6

Note: c = coefficient of the damping elements; k = stiffness coefficient of the spring elements; m = mass of the related body segments.

Appendix 2

Equations of motion of Model 1

$$m_1\ddot{z}_1 + c_1(\dot{z}_1 - \dot{z}_0) + c_2(\dot{z}_1 - \dot{z}_2) + k_1(z_1 - z_0) + k_2(z_1 - z_2) = 0, \quad \text{(B.1)}$$

$$m_2\ddot{z}_2 + c_2(\dot{z}_2 - \dot{z}_1) + c_3(\dot{z}_2 - \dot{z}_3) + k_2(z_2 - z_1) + k_3(z_2 - z_3) = 0, \quad \text{(B.2)}$$

$$m_3\ddot{z}_3 + c_3(\dot{z}_3 - \dot{z}_2) + c_4(\dot{z}_3 - \dot{z}_4) + k_3(z_3 - z_2) + k_4(z_3 - z_4) = 0, \quad \text{(B.3)}$$

$$m_4\ddot{z}_4 + c_4(\dot{z}_4 - \dot{z}_3) + k_4(z_4 - z_3) = 0, \quad \text{(B.4)}$$

where c = coefficient of the damping elements; k = stiffness coefficient of the spring elements; m = mass of the related body segments; z = displacement of the related body segment; z_0 = displacement of the seat pad; $\dot{z}_0$ = velocity of the seat pad; $\ddot{z}_0$ = acceleration of the seat pad.

Equations of motion of Model 2

$$m_1\ddot{z}_1 + c_1(\dot{z}_1 - \dot{z}_0) + c_2(\dot{z}_1 - \dot{z}_2) + c_3(\dot{z}_1 - \dot{z}_3) + k_1(z_1 - z_0) + k_2(z_1 - z_2) + k_3(z_1 - z_3) = 0, \quad \text{(B.5)}$$

$$m_2\ddot{z}_2 + c_2(\dot{z}_2 - \dot{z}_1) + c_4(\dot{z}_2 - \dot{z}_4) + k_2(z_2 - z_1) + k_4(z_2 - z_4) = 0, \quad \text{(B.6)}$$

$$m_3\ddot{z}_3 + c_3(\dot{z}_3 - \dot{z}_1) + c_7(\dot{z}_3 - \dot{z}_7) + k_3(z_3 - z_1) + k_7(z_3 - z_7) = 0, \quad \text{(B.7)}$$

$$m_4\ddot{z}_4 + c_4(\dot{z}_4 - \dot{z}_2) + c_5(\dot{z}_4 - \dot{z}_5) + k_4(z_4 - z_2) + k_5(z_4 - z_5) = 0, \quad \text{(B.8)}$$

$$m_5\ddot{z}_5 + c_5(\dot{z}_5 - \dot{z}_4) + c_6(\dot{z}_5 - \dot{z}_6) + k_5(z_5 - z_4) + k_6(z_5 - z_6) = 0, \quad \text{(B.9)}$$

$$m_6\ddot{z}_6 + c_6(\dot{z}_6 - \dot{z}_5) + c_{67}(\dot{z}_6 - \dot{z}_7) + c_8(\dot{z}_6 - \dot{z}_8) + k_6(z_6 - z_5) + k_{67}(z_6 - z_7) + k_8(z_6 - z_8) = 0, \quad \text{(B.10)}$$

$$m_7\ddot{z}_7 + c_{67}(\dot{z}_7 - \dot{z}_6) + c_7(\dot{z}_7 - \dot{z}_3) + c_{10}(\dot{z}_7 - \dot{z}_{10}) + k_{67}(z_7 - z_6) + k_7(z_7 - z_3) + k_{10}(z_7 - z_{10}) = 0, \quad \text{(B.11)}$$

$$m_8\ddot{z}_8 + c_8(\dot{z}_8 - \dot{z}_6) + c_9(\dot{z}_8 - \dot{z}_9) + k_8(z_8 - z_6) + k_9(z_8 - z_9) = 0, \quad \text{(B.12)}$$

$$m_9\ddot{z}_9 + c_9(\dot{z}_9 - \dot{z}_8) + k_9(z_9 - z_8) = 0, \quad \text{(B.13)}$$

$$m_{10}\ddot{z}_{10} + c_{10}(\dot{z}_{10} - \dot{z}_7) + c_{11}(\dot{z}_{10} - \dot{z}_{11}) + k_{10}(z_{10} - z_7) + k_{11}(z_{10} - z_{11}) = 0, \quad \text{(B.14)}$$

$$m_{11}\ddot{z}_{11} + c_{11}(\dot{z}_{11} - \dot{z}_{10}) + k_{11}(z_{11} - z_{10}) = 0, \quad \text{(B.15)}$$

where c = coefficient of the damping elements; k = stiffness coefficient of the spring elements; m = mass of the related body segments; z = displacement of the related body segment; z_0 = displacement of the seat pad; $\dot{z}_0$ = velocity of the seat pad; $\ddot{z}_0$ = acceleration of the seat pad.